Report

Current Biology

Termination of Protofilament Elongation by Eribulin Induces Lattice Defects that Promote Microtubule Catastrophes

Highlights

- Eribulin binds to a site on β-tubulin, which is exposed at microtubule plus ends
- Single Eribulin molecules induce erratic microtubule plus-end growth and catastrophes
- Eribulin induces EB3 comet splitting
- Eribulin amplifies a natural pathway of catastrophe induction

Authors

Harinath Doodhi, Andrea E. Prota, Ruddi Rodríguez-García, ..., Lukas C. Kapitein, Anna Akhmanova, Michel O. Steinmetz

Correspondence

l.kapitein@uu.nl (L.C.K.), a.akhmanova@uu.nl (A.A.), michel.steinmetz@psi.ch (M.O.S.)

In Brief

Doodhi et al. show that Eribulin binds to a site on β-tubulin, which is exposed at the plus ends of microtubules. Binding of single Eribulin molecules induces erratic microtubule growth, catastrophes, and splitting of EB3 comets. The authors propose that Eribulin amplifies a natural catastrophe pathway by inhibiting protofilament elongation.

Accession Numbers

5JH7

Doodhi et al., 2016, Current Biology *26*, 1713–1721
July 11, 2016
http://dx.doi.org/10.1016/j.cub.2016.04.053

CellPress

Current Biology
Report

Termination of Protofilament Elongation by Eribulin Induces Lattice Defects that Promote Microtubule Catastrophes

Harinath Doodhi,[1,6,7] Andrea E. Prota,[2,6] Ruddi Rodríguez-García,[1,6] Hui Xiao,[3] Daniel W. Custar,[4] Katja Bargsten,[2,8] Eugene A. Katrukha,[1] Manuel Hilbert,[2,9] Shasha Hua,[1] Kai Jiang,[1] Ilya Grigoriev,[1] Chia-Ping H. Yang,[3] David Cox,[5,10] Susan Band Horwitz,[3] Lukas C. Kapitein,[1,*] Anna Akhmanova,[1,*] and Michel O. Steinmetz[2,*]
[1]Cell Biology, Department of Biology, Faculty of Science, Utrecht University, 3584 CH Utrecht, the Netherlands
[2]Laboratory of Biomolecular Research, Department of Biology and Chemistry, Paul Scherrer Institut, 5232 Villigen, Switzerland
[3]Department of Molecular Pharmacology, Albert Einstein College of Medicine, Bronx, NY 10461, USA
[4]Oncology PCU, Eisai Product Creation Systems, Eisai, Andover, MA 01810, USA
[5]Medical Affairs, Eisai Global Oncology Business Unit, Eisai, Woodcliff Lake, NJ 07677, USA
[6]Co-first author
[7]Present address: Centre for Gene Regulation and Expression, School of Life Sciences, University of Dundee, Dow Street, Dundee DD1 5EH, UK
[8]Present address: Institute of Biochemistry, University of Zürich, 8006 Zürich, Switzerland
[9]Present address: Roche Pharma Research and Early Development, Chemical Biology, Roche Innovation Center Basel, F. Hoffmann-La Roche, 4000 Basel, Switzerland
[10]Present address: Medical Affairs, Ipsen Biopharmaceuticals, Basking Ridge, NJ 07920, USA
*Correspondence: l.kapitein@uu.nl (L.C.K.), a.akhmanova@uu.nl (A.A.), michel.steinmetz@psi.ch (M.O.S.)
http://dx.doi.org/10.1016/j.cub.2016.04.053

SUMMARY

Microtubules are dynamic polymers built of tubulin dimers that attach in a head-to-tail fashion to form protofilaments, which further associate laterally to form a tube. Asynchronous elongation of individual protofilaments can potentially lead to an altered microtubule-end structure that promotes sudden depolymerization, termed catastrophe [1–4]. However, how the dynamics of individual protofilaments relates to overall growth persistence has remained unclear. Here, we used the microtubule targeting anti-cancer drug Eribulin [5–7] to explore the consequences of stalled protofilament elongation on microtubule growth. Using X-ray crystallography, we first revealed that Eribulin binds to a site on β-tubulin that is required for protofilament plus-end elongation. Based on the structural information, we engineered a fluorescent Eribulin molecule. We demonstrate that single Eribulin molecules specifically interact with microtubule plus ends and are sufficient to either trigger a catastrophe or induce slow and erratic microtubule growth in the presence of EB3. Interestingly, we found that Eribulin increases the frequency of EB3 comet "splitting," transient events where a slow and erratically progressing comet is followed by a faster comet. This observation possibly reflects the "healing" of a microtubule lattice. Because EB3 comet splitting was also observed in control microtubules in the absence of any drugs, we propose that Eribulin amplifies a natural pathway toward catastrophe by promoting the arrest of protofilament elongation.

RESULTS AND DISCUSSION

Crystal Structure of the Tubulin-Eribulin Complex

To investigate the molecular mechanism of action of Eribulin on tubulin and microtubules, we soaked crystals of a protein complex composed of two αβ-tubulin heterodimers (T_2), the stathmin-like protein RB3 (R) and tubulin tyrosine ligase (TTL) [8, 9] with Eribulin (Figure 1A), and determined the tubulin-bound structure of the drug by X-ray crystallography at 2.2 Å resolution (Figures 1B and S1A; Table S1). Eribulin bound to the so called vinca domain at the inter-dimer interface between two longitudinally aligned tubulin dimers [10, 11] (Figure 1C), consistent with previous biochemical information [6, 12–14]. However, Eribulin also interacted in a similar manner with the exposed β-tubulin subunit of the second tubulin dimer in the T_2R-TTL complex (Figures 1B and S1A). To probe the tubulin-Eribulin interaction in solution, we performed hydrogen deuterium exchange experiments in combination with mass spectrometry (HDX-MS). As shown in Figure 1D, little change was seen in α-tubulin upon Eribulin binding to unassembled tubulin. In contrast, Eribulin protected four peptides, 74–111, 128–151, 167–187 and 212–230, of β-tubulin from hydrogen deuterium exchange (Figures 1D and S1B). These data suggest that Eribulin binds predominantly to half of the vinca domain on β-tubulin.

Eribulin is engaged with both common and unique structural elements compared to the archetypical vinca-site ligand Vinblastine (Figure 1C). Its binding site is shaped by hydrophobic and polar residues of helices H1, H6, and H7 and loops H6-H7, S3-H3′ (T3), and S5-H5 (T5) of β-tubulin (Figure 1E), which is consistent with our HDX-MS data. In addition, the "cage"

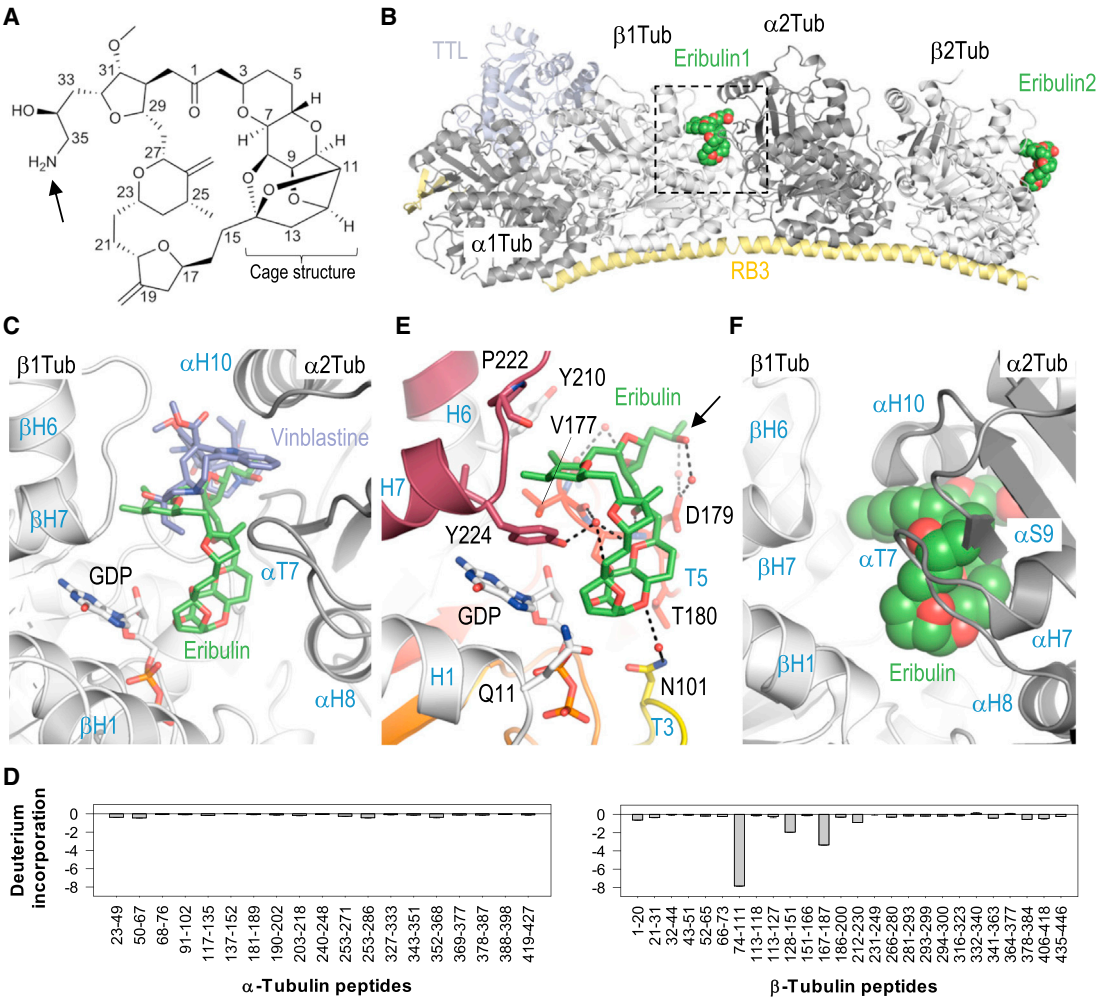

Figure 1. Tubulin-Eribulin Complex Structure

(A) Chemical structure of Eribulin.

(B) Overall view of the T_2R-TTL-Eribulin complex. Tubulin (gray), RB3 (yellow), and TTL (blue) are shown in ribbon representation; Eribulin is depicted in green spheres representation. The dashed box highlights the area shown in (C).

(C) Close-up view of the superimposition of the tubulin-Eribulin and tubulin-Vinblastine (PDB ID 4EB6) complex structures. α- and β-tubulin are shown as dark and light gray ribbon representations, respectively. Eribulin, Vinblastine, and GDP are depicted in green, blue, and gray sticks representation, respectively.

(D) Drug-induced alterations in deuteration referenced against chicken erythrocyte tubulin for α-tubulin (left) and β-tubulin (right). Differences in deuteration (ΔHDX) are expressed in Da. Peptides are labeled with the corresponding amino acid numbers in the sequences of α- and β-tubulin. Error bars represent SD (n = 3 experiments)

(E) Close-up view of the tubulin-Eribulin interaction (same view as in C). Eribulin is in green sticks representation; β-tubulin is displayed as gray ribbon. Key residues forming the interaction with the ligand are in sticks representation. Oxygen and nitrogen atoms are colored in red and blue, respectively; carbon atoms of Eribulin in green. Carbon atoms of β-tubulin are colored according to the segments identified by HDX MS (see D): 74–111, yellow; 128–151, orange; 167–187, red; 212–230, raspberry; all other residues, gray. Hydrogen bonds are depicted as black dashed lines; water molecules are indicated as red spheres. In the tubulin-Eribulin complex, the ligand wraps around the side chain of Tyr224; its CO3 and CO8 groups establish a prominent water-mediated hydrogen bonding interaction network with the OH group of the side chain of Tyr224 and with the main chain carbonyl group of Val177 of β-tubulin. Additional hydrogen bonds are observed between the CO1 group and the main chain of Asp179 (direct), between the CO10 group and the side chain of Asn101 (water mediated), between the O31 atom and the main chain of Lys176 (water mediated), and between the OH34 and H_2N35 groups and the side chain of Asp179 (water mediated) of Eribulin and β-tubulin, respectively.

(F) Close-up view of the tubulin-Eribulin interaction in the context of a microtubule (PDB ID 3J6G). The β1- and α2-tubulin chains are displayed in light and dark gray ribbons, respectively. The ligand is in green spheres representation.

The arrows in (A) and (E) point to the site in Eribulin to which the Alexa 488 fluorophore has been attached. See also Figure S1 and Table S1.

structure of Eribulin (Figure 1A) is in contact with the ribose moiety of the guanosine nucleotide. It seems to act as a molecular "lid" that could inhibit nucleotide exchange and tubulin-tubulin-induced hydrolysis (Figure S1C), in agreement with biochemical data [12–14]. In the tubulin-Eribulin complex, the ligand wraps around the side chain of Tyr224.

The curved structure of tubulin in the T_2R-TTL complex corresponds to the conformation of unassembled tubulin [15, 16].

However, tubulin undergoes a "curved-to-straight" conformational transition upon assembly into microtubules [17]. We found that the overall architecture of the Eribulin-binding site is only marginally affected by the curved-to-straight structural rearrangements (Figures S1D and S1E). This analysis indicates that Eribulin should also be able to interact with tubulin in the straight conformational state. We also investigated Eribulin binding in the context of two longitudinally aligned tubulin dimers as found in microtubules: as shown in Figure 1F, we found that the strand S9, helix H10, and loop T7 of α-tubulin from the neighboring tubulin dimer would clash into the main body of the Eribulin molecule.

These results suggest that Eribulin can sequester tubulin dimers into assembly incompetent tubulin-Eribulin complexes. However, they further indicate that the drug could also bind β-tubulin subunits exposed at distal microtubule plus ends, which is expected to effectively inhibit or even terminate protofilament elongation. Notably, the mechanism of action of Eribulin is different from that of Vinblastine, which induces tubulin ring-like oligomer formation due to the binding of the drug to the full vinca domain that is shaped by residues stemming from both α- and β-tubulin subunits [10, 12]. The mode of action of Eribulin is, however, similar to the clinically relevant microtubule-destabilizing agent Maytansine that binds to a site on β-tubulin that is distinct from the vinca domain but also located at the longitudinal interface between tubulin dimers in microtubules [18]. In addition, the binding site of Eribulin overlaps with the one of DARPin D1, a designed ankyrin-repeat protein that caps microtubule plus ends and induces their disassembly [16].

Design and Characterization of a Fluorescently Labeled Eribulin Derivative

To test the predictions that emerged from our structural data, we synthesized a fluorescent Eribulin derivative in which an Alexa 488 fluorophore was attached to the H_2N35 group of the drug (Eribulin-A488; Figure S2A). Based on the tubulin-Eribulin complex structure, we reasoned that the addition of a large chemical entity to the H_2N35 group of Eribulin should not significantly affect the tubulin-binding properties of the drug, as this site is located at a distance from the β-tubulin surface and points into solution (see arrow in Figure 1E). The affinity of Eribulin-A488 for tubulin was assessed by fluorescence anisotropy titration experiments, which revealed an equilibrium dissociation constant, K_D, of 34 ± 3 nM (Figure S2B). The affinity of unmodified Eribulin was subsequently determined as 45 ± 15 nM by a competition experiment (Figure S2B). These results show that Eribulin binds with high affinity to unassembled tubulin and that the fluorophore in Eribulin-A488 does not significantly interfere with the binding activity of the drug. Notably, a previous study reported the binding of [3H]Eribulin to tubulin using a centrifugal gel-filtration assay [6]. This study revealed that Eribulin binds to a single site on β-tubulin with an overall K_D of 46 μM but also shows a high-affinity interaction with a K_D of 0.4 μM for a subset of tubulin dimers. The difference between our results and the previous study is likely due to the very different assay systems used.

We next assessed whether Eribulin-A488 binds specifically to microtubule plus ends. We found that Eribulin-A488 (1–10 μM) indeed localized only to one end of GMPCPP- or Taxol-stabilized microtubules (Figures 2A and 2B), which was identified as the plus end by using microtubule gliding assays with the plus-end-directed motor kinesin-1 (Figure S2C). To quantify the fluorescence signals at microtubule ends, we used the averaged intensity of single Eribulin-A488 molecules that were non-specifically bound to the coverslip as a reference (Figures S2D–S2G). We estimated that an average of approximately four fluorescent Eribulin molecules localized to a single microtubule end if the drug was washed away before imaging (Figure 2C) and approximately ten molecules if the microtubules were imaged directly (Figure S2H). Given that after spontaneous nucleation microtubules in vitro are composed of 11–17 protofilaments [19], these data suggest that the majority of the protofilaments have at most one single Eribulin molecule bound to their exposed β-tubulin subunit at distal microtubule plus ends.

Effects of Eribulin-A488 on Microtubule Dynamics

The effect of Eribulin-A488 on microtubule dynamics was tested using a total internal reflection fluorescence (TIRF) microscopy-based microtubule dynamics reconstitution assay [20, 21]. As shown in Figures 2D and 2E, 500 nM Eribulin strongly slows down the microtubule growth rate at plus ends without significantly affecting the catastrophe frequency. In contrast, the microtubule minus-end growth rate was not affected (Figure 2F). However, minus ends displayed substantial pausing, which strongly complicated the reliable quantification of catastrophes (Figure 2D). We thus cannot exclude that in the conditions tested Eribulin affects microtubule minus-end dynamics to some extent, but the drug certainly did not inhibit minus-end elongation.

Next, we examined the effect of Eribulin on microtubules grown in the presence of mCherry-labeled EB3 (mCherry-EB3) [22]. Our previous work has shown that EBs sensitize microtubule plus ends to the action of microtubule-targeting agents by promoting catastrophes [21]. Similarly, we found that in the presence of mCherry-EB3, 50–100 nM Eribulin had a significant catastrophe-promoting effect at the plus end (Figures 2G and 2H), while five to ten times higher drug concentrations were needed to induce a profound effect on microtubule plus-end dynamics (reduction of growth rate) in the absence of mCherry-EB3 (Figures 2D and 2E). The EB-induced catastrophe enhancement could be explained by the fact that EBs accelerate GTP hydrolysis and/or promote structural changes at growing microtubule tips [23, 24]. At 500 nM or higher Eribulin concentrations, microtubules imaged in the presence of mCherry-EB3 failed to elongate due to very frequent catastrophes (data not shown); however, at 250 nM Eribulin, some microtubule plus-end growth was observed both with and without mCherry-EB3 (Figures 2E and 2H), thus allowing for a direct comparison. With tubulin alone, a mild reduction of the microtubule growth rate was observed in these conditions, while the catastrophe frequency was not affected (Figures 2D and 2E). In the presence of mCherry-EB3, the microtubule growth rate was reduced and the catastrophe frequency increased almost 3-fold (Figures 2G and 2H). Microtubule minus-end dynamics was not significantly affected in the presence of mCherry-EB3 and 250 nM Eribulin (Figure 2I). Importantly, we found that the effects of Eribulin and Eribulin-A488 on microtubule dynamics were very similar, indicating that the addition of the fluorescent label did not significantly affect the properties of the drug (Figures 2E–2I).

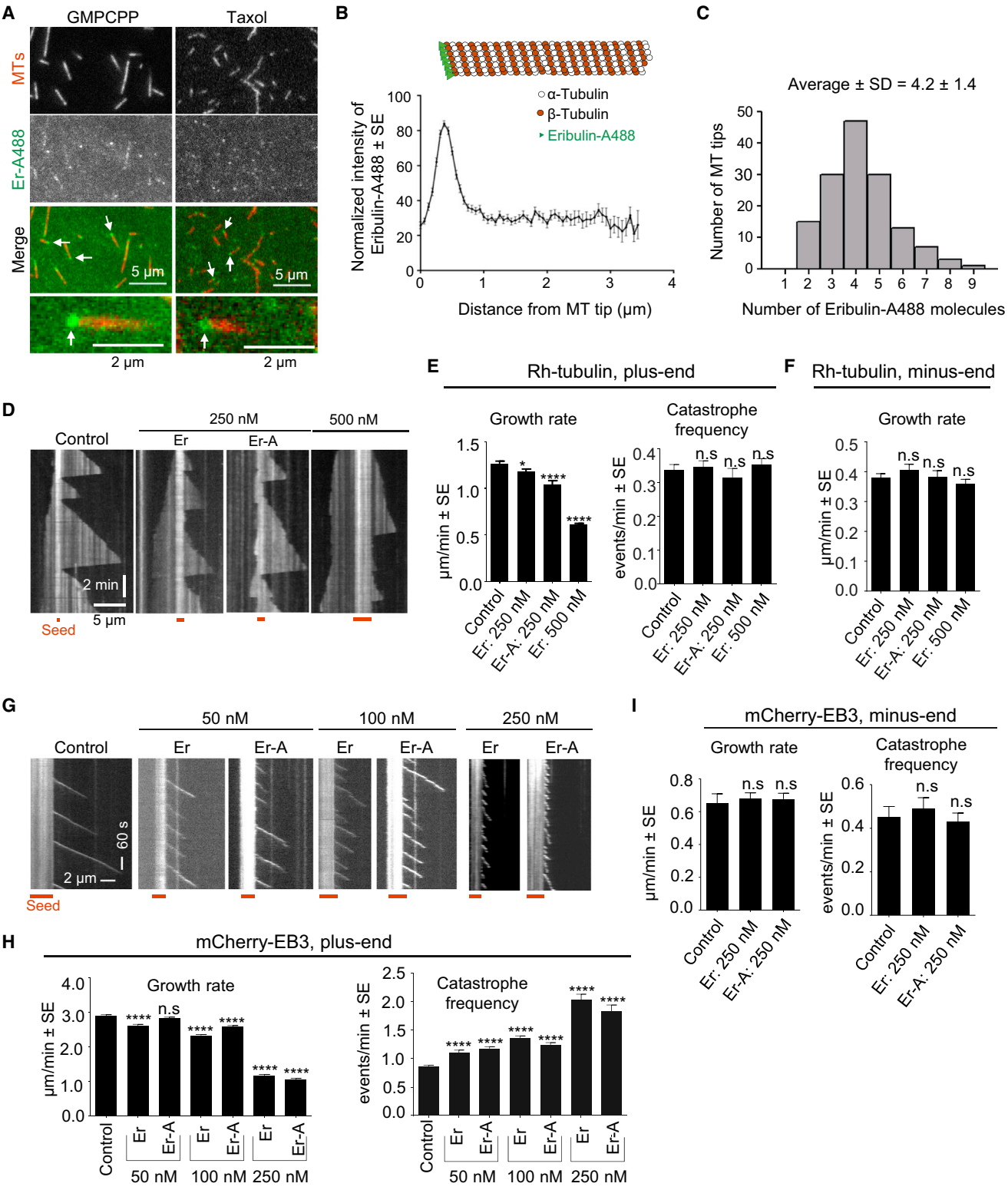

Figure 2. Effects of Eribulin on Microtubule Dynamics

(A) GMPCPP- or Taxol-stabilized microtubules that were incubated with Eribulin-A488 (10 μM) and which were subsequently separated from the excess of the drug by pelleting. Distinct localization of Eribulin-A488 to only one end of the microtubule is observed (arrows); enlargements are shown at the bottom.

(B) Quantification of the intensity of Eribulin-A488 along the length of GMPCPP-stabilized microtubules (n = 146).

(C) Quantification of the number of Eribulin-A488 molecules at the tip of GMPCPP-stabilized microtubules (n = 146).

(legend continued on next page)

The impact of Eribulin on in vitro microtubule plus-end dynamics in the presence of mCherry-EB3 is similar to that observed in cells: 20 nM Eribulin decreased the microtubule growth rate by ~20%, increased the catastrophe frequency by ~2.5-fold, and thus strongly reduced the length of microtubule growth episodes; at 50 nM Eribulin, microtubule growth was almost completely stalled (Figures S2I and S2J). These results demonstrate that Eribulin potently inhibits microtubule plus-end growth, in agreement with previous studies [5–7], and that the catastrophe-inducing effect of Eribulin in cells can be reconstituted in vitro in the presence of EB3.

Eribulin Induces Microtubule Lattice Defects

The data collected thus far suggest that Eribulin-A488 can be used to perturb plus-end growth of individual protofilaments of a microtubule. To test this possibility, we focused on microtubules assembled in the presence of mCherry-EB3 because their growth was already affected by 50 nM of drug, a concentration at which the background fluorescence was sufficiently low for the imaging of single molecules. Using dual-color imaging with Eribulin-A488 and mCherry-EB3, we detected distinct drug binding events at microtubule plus ends (Figures 3A and 3B). These events corresponded to transient immobilization of single Eribulin-A488 molecules, as demonstrated by quantification of fluorescence intensities (Figure 3C). The residence times of Eribulin-A488 on microtubule plus ends were exponentially distributed with a mean value of 4.0 ± 0.5 s (n = 120) (Figure 3D). In 29% of cases, the interaction of Eribulin-A488 with microtubule plus ends was followed by a catastrophe within a period of 0 to 5 s (n = 111). In the remaining cases, the microtubules continued growing and extended up to ~3.5 μm in length after an Eribulin-A488 molecule bound to the microtubule tip (Figures 3E and 3F); however, both the overall growth length and the growth duration were significantly shorter compared to microtubules that were not targeted by the drug in the same assay (Figures S3A–S3D). Importantly, microtubule growth beyond the Eribulin binding site was invariably perturbed: the rate of microtubule growth was reduced by ~33% (Figure 3G) and the intensities of mCherry-EB3 plus-end comets dropped almost immediately after Eribulin-A488 binding (Figures 3H and S3E). Such a reduction in intensity could be simply due to the slower microtubule growth rate [20]; however, perturbation of the microtubule plus-end structure upon drug binding might also contribute to the reduced mCherry-EB3 signal. Indeed, the mCherry-EB3 signal after Eribulin binding was often less continuous than during normal microtubule growth (Figures 3A and 3B).

To confirm these observations, we investigated the distribution of mCherry-EB3 comet intensities during growth frame-by-frame in the presence and absence of 200 nM Eribulin, the concentration at which microtubule growth episodes are strongly affected but nevertheless long enough to be observable (Figures S3F–S3H). We found that EB3 intensities were strongly shifted toward lower values, corresponding to the frequent temporary loss of the mCherry-EB3 signal. This result cannot be explained by a slower microtubule growth rate because microtubules assembled in the presence of reduced tubulin concentrations, which elongated even slower, did not show interrupted mCherry-EB3 signals (Figures S3F–S3H). These data suggest that Eribulin binding to microtubule plus ends does not simply slow down tubulin addition but also has an effect on the microtubule tip structure.

To further assess the microtubule elongation process upon Eribulin binding, we quantified the straightness index of microtubule tip growth, which is the ratio between the start-to-end displacement of a microtubule tip and the total length of the path that the tip has traveled [25]. We found that the straightness index was reduced by ~0.2 after Eribulin binding to a growing microtubule tip, while a reduction of not more than ~0.02 could be expected based on the extent of microtubule elongation within the 10-s period of a measurement (Figures 3I and S3I). This result could not be explained by the reduction in microtubule growth velocity since a similar ~30% reduction in microtubule polymerization rate obtained by decreasing the tubulin concentration did not affect the straightness index (Figures S3G and S3J). Instead, these results indicate that the binding of a single Eribulin molecule induces slow and erratic microtubule plus-end growth that deviates from a straight path, suggesting an alteration in the mechanical properties of the microtubule. Based on these observations and on our structural data indicating that Eribulin is expected to prevent protofilament elongation, we propose that Eribulin binding induces protofilament loss and a lattice defect, such as the formation of an incomplete, more flexible tube, which can propagate for several micrometers.

Repair of Eribulin-Induced Microtubule Lattice Defects

We next sought to investigate whether an Eribulin-induced lattice defect can be repaired. Indeed, such an event is shown in Figures 3B (event 6; enlarged in Figure 4A): after Eribulin binding, the growth of the mCherry-EB3 comet slowed down and became less intense, while a second, faster growing comet emerged from the site of Eribulin binding after the drug dissociated. This "rear comet" eventually caught up and fused with the "leading comet" (Figure 4A). We found that 150 nM of Eribulin was optimal to observe such comet "splitting" events. Importantly, analysis of mCherry-EB3-labeled microtubule tips revealed that split comets can also be observed in the absence of Eribulin, although with a greatly reduced frequency compared to the ones imaged in the presence of the drug (Figures 4B–4D).

(D and G) Representative kymographs illustrating the dynamics of microtubules grown in the presence of rhodamine-tubulin (D) or mCherry-EB3 (G) at different concentrations of Eribulin. The red lines at the bottom of the kymographs indicate GMPCPP-stabilized rhodamine microtubule seeds. Microtubule plus ends point to the right.

(E and F) Microtubule plus-end growth rates (E, left) and catastrophe frequencies (E, right), and minus-end growth rates (F) obtained in the presence of rhodamine-tubulin at various concentrations of Eribulin or Eribulin-A488.

(H and I) Microtubule plus-end growth rates (H, left) and catastrophe frequencies (H, right), and minus-end growth rates (I) obtained in the presence of mCherry-EB3 at different concentrations of Eribulin or Eribulin-A488. (*p < 0.0, ****p < 0.0001; n.s., not significant, p > 0.05; Mann-Whitney two-tailed test.)

MT, microtubule; Rh-tubulin, rhodamine-tubulin; Er, Eribulin; Er-A, Eribulin-A488. See also Figures S2 and S3.

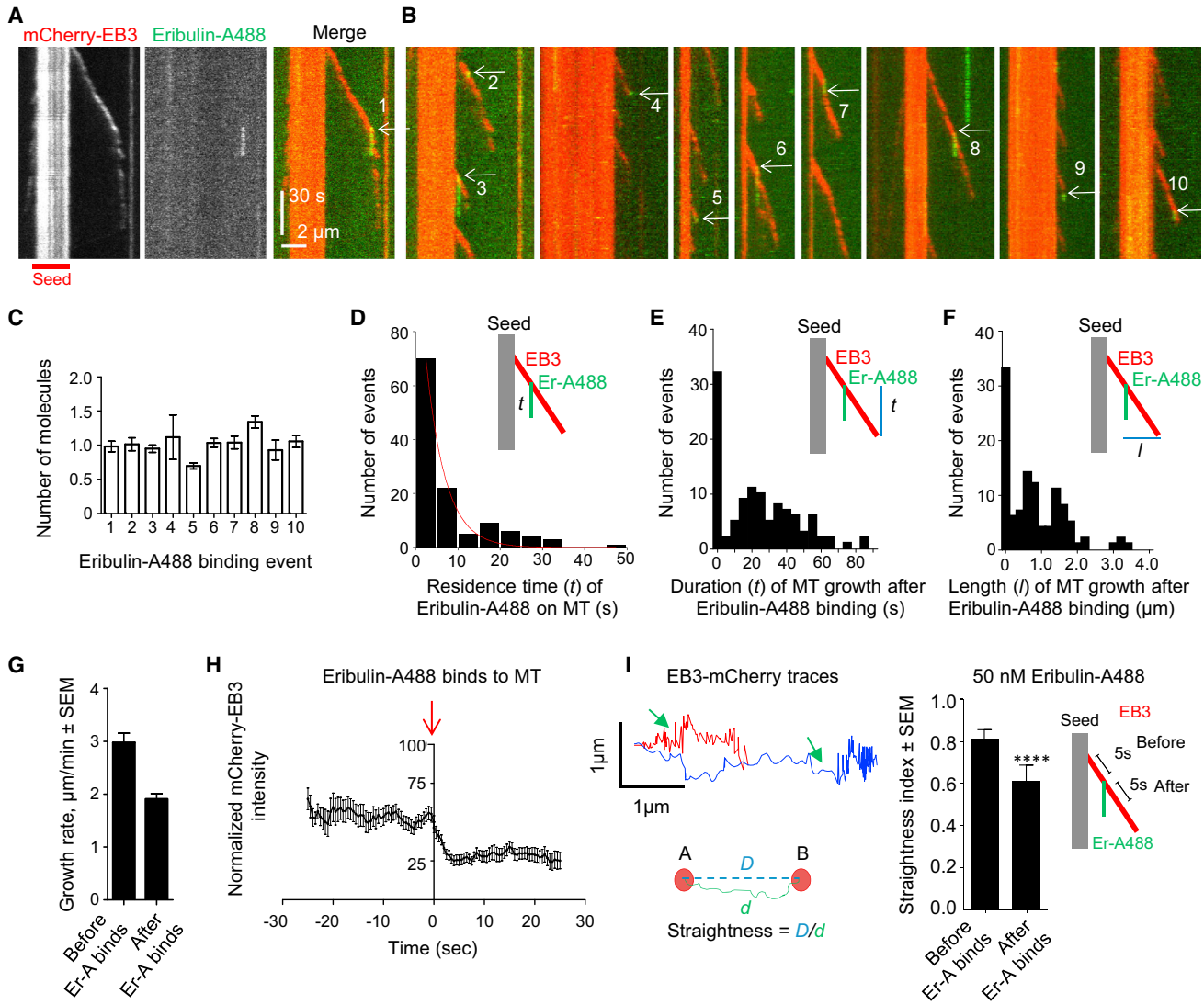

Figure 3. Effects of Single Eribulin-A488 Molecules on Growing Microtubule Plus Ends

(A and B) Kymographs illustrating Eribulin-A488 binding events (arrows) to growing microtubule tips visualized with mCherry-EB3.

(C) Quantification of the number of Eribulin-A488 molecules on dynamic microtubules from the ten different binding events shown in (A and B). Error bars represent SEM; averaged over the number of frames, which varied from 5 to 35.

(D) Distribution of residence times of Eribulin-A488 on dynamic microtubules (n = 120).

(E) Distribution of durations of microtubule growth times after an Eribulin-A488 binding event occurred (n = 111).

(F) Distribution of microtubule growth lengths after an Eribulin-A488 binding event (n = 111).

(G) Microtubule growth rates before and after Eribulin-A488 binding to growing microtubules (n = 31).

(H) Normalized intensities of mCherry-EB3, ~25 s before and after Eribulin-A488 binding to microtubules (n = 31).

(I) Top left: examples of two EB3 comet traces, with Eribulin binding events indicated by arrows. Bottom left: a scheme illustrating the measurement of the straightness index. Right: the straightness index for microtubule growth before and after Eribulin-A488 binding (n = 12) (****$p < 0.0001$; Mann-Whitney two-tailed test).

MT, microtubule; Er, Eribulin; Er-A, Eribulin-A488. See also Figures S3 and S4.

The average length traveled by the rear comet during catching-up episodes was 0.5 ± 0.1 μm. Comet splitting events were always accompanied by a reduction in the growth speed of the leading comet and the emergence of a much faster rear comet, which eventually fused with the leading one (Figures 4A–4E). Furthermore, the intensities of both the leading and the rear comets were always lower than the ones observed either before the initial comet splitting or after their merge (Figure 4E). This result suggests that both the leading and rear comets contain only a subset of protofilaments. The brightness of an EB comet depends on the growth rate [20] and the number of protofilaments [26], which together define the number of EB-binding sites. Since the rear comet always moved faster than the leading one but the intensities of both comets after splitting were comparable (Figure 4E), it is likely that the rear comet contained fewer protofilaments than the leading one. Additionally, the straightness index of the leading

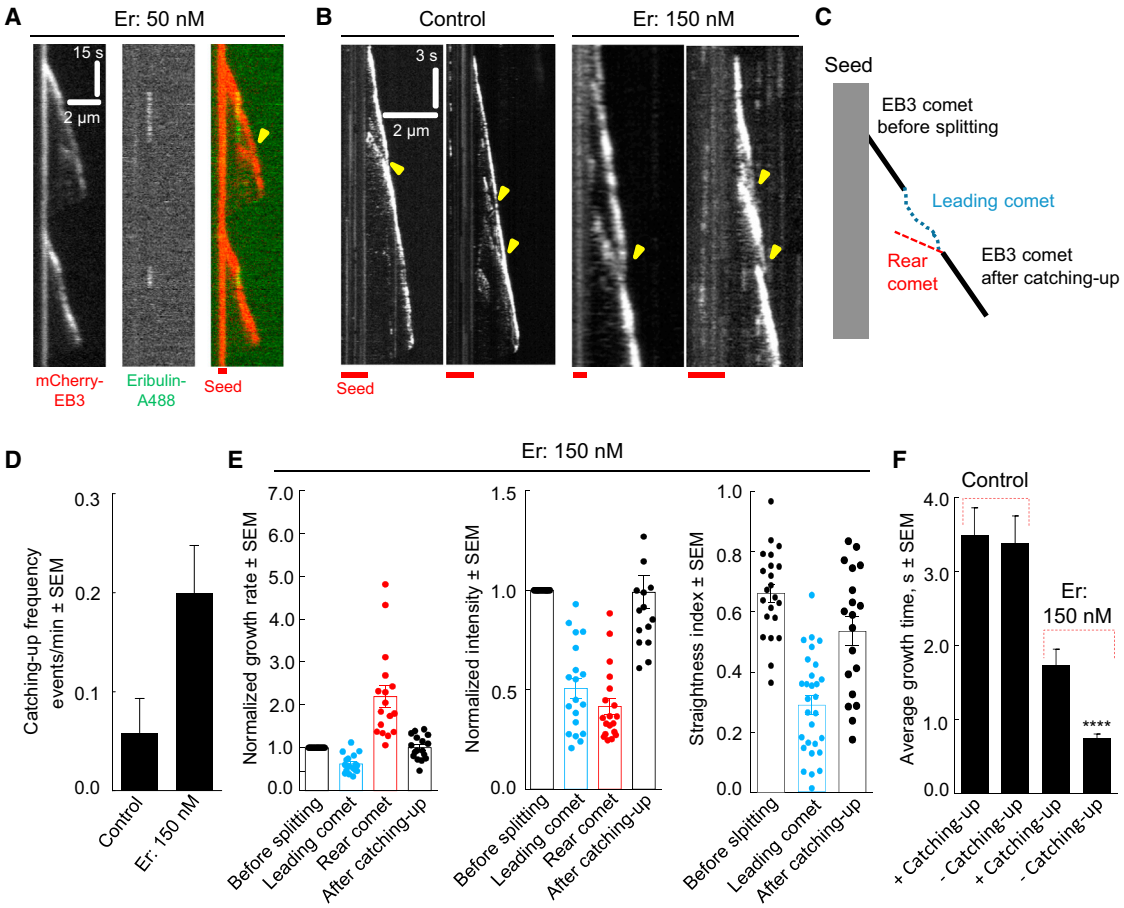

Figure 4. Analysis of Eribulin-Induced Split EB3 Comets

(A and B) Kymographs illustrating the emergence of a catching-up comet visualized with mCherry-EB3 (yellow arrowheads), either after binding and detachment of a single Eribulin-A488 molecule (A; 50 nM Eribulin-A488) or in control microtubules (B, left) and microtubules grown in the presence of 150 nM of unlabeled Eribulin (B, right).

(C) Schematic representation of an EB3 comet catching-up episode.

(D) Frequency of catching-up events in control and in the presence of 150 nM Eribulin. The frequency was computed by dividing the number of catching-up events by the total growth time. 25–28 events were analyzed per condition.

(E) Quantification of growth rates, comet intensities, and straightness indexes for the four periods of a catching-up event defined in (C). The data were obtained in the presence of 150 nM Eribulin. Straightness indexes were calculated by using tracks of 0.3 s in each episode of the event. The values of intensities and growth rates were normalized to the values of the comets before the splitting (n = 19).

(F) Average growth time of microtubules with at least one catching-up episode, compared to the average growth time of microtubules without undergoing such an event. The analysis was done in the absence (control) and presence of 150 nM Eribulin (n = 25–74 per condition).

comet was significantly lower than that of the comet observed before the splitting event and correlated with the intensity of the comet (Figures 4E and S4A). This reduction of the straightness index was not due to a reduced precision of the localization of comet tips (Figure S4B). These findings suggest that the leading comet of a split event represents the elongation of a defective microtubule plus end that is more flexible. In line with this view, the straightness index increased approximately to the initial value after the rear comet caught up with the leading one (Figure 4E). This result suggests that the fusion of the two comets reflects the restoration of the microtubule tip structure that has been perturbed due to Eribulin binding. Consistent with this hypothesis, we found that at 150 nM Eribulin microtubules featuring catching-up events grew on average longer than microtubules without such events (Figure 4F). We did not detect a similar dependence in microtubules imaged in the absence of Eribulin (Figure 4F), most likely because catching-up events in such conditions are rare.

Based on the results obtained in the presence of Eribulin, we reasoned that if catching-up events represent rescues of growing microtubules that were on a path toward a catastrophe, then the properties of the leading comets during such events might be similar to those of control microtubules that are in a pre-catastrophe state. Previous work showed that the EB comet intensity is gradually reduced before a catastrophe occurs [26, 27]. We confirmed this observation, but also found that the microtubule growth velocity and the straightness index were both gradually reduced during the ~10-s period preceding a catastrophe (Figure S4C). This observation suggests that the properties of a microtubule plus end that is in a pre-catastrophe state are similar to those of a microtubule tip whose proper

elongation is perturbed by a drug that inhibits protofilament elongation.

Conclusions

Our data suggest that Eribulin can destabilize microtubules or suppress microtubule dynamics by either sequestering tubulin dimers into assembly-incompetent tubulin-drug complexes at high drug concentrations, or by perturbing protofilament elongation at microtubule plus ends at low drug concentrations. In the latter case, we favor the idea that Eribulin physically blocks a protofilament end; however, alternative models involving more complex perturbations of the microtubule-end structure cannot be ruled out at this stage. Interestingly, we also occasionally observed indications of protofilament blocking in control microtubules in the absence of any drugs, an effect that could contribute to naturally occurring catastrophes. Previous work has shown that the catastrophe frequency might reflect the accumulation of structural defects, such as plus-end tapering due to asynchronously growing protofilaments [1–4]. Strikingly, we found that the behavior of a pre-catastrophe microtubule tip in control microtubules is similar to the ones that are expected to lack protofilaments after Eribulin binding: in both cases the growth rate, the EB3 comet intensity and the straightness index were reduced. Therefore, it is tempting to propose that lagging protofilaments represent a pathway toward microtubule catastrophe, and it is possible that EB proteins affect this pathway by influencing the stability of the microtubule-end structure that lacks protofilaments. In conclusion, our approach represents a general strategy to investigate and manipulate the dynamics of cytoskeletal arrays at high resolution. In addition, it provides a unique way to directly visualizing individual therapeutically relevant microtubule-targeting drugs as they interact with their molecular target.

ACCESSION NUMBERS

The accession number for the coordinates of the T_2R-TTL-Eribulin complex reported in this paper is Protein Data Bank (PDB): 5JH7.

SUPPLEMENTAL INFORMATION

Supplemental Information includes Supplemental Experimental Procedures, four figures, and one table and can be found with this article online at http://dx.doi.org/10.1016/j.cub.2016.04.053.

AUTHOR CONTRIBUTIONS

H.D., A.E.P., R.R.-G., H.X., D.W.C., E.A.K., M.H., D.C. S.B.H., L.C.K., A.A., and M.O.S. designed the experiments. H.D., A.E.P., R.R.-G., H.X., D.W.C., K.B., M.H., S.H., K.J., I.G., and C.-P.H.Y conducted the experiments. H.D., A.E.P., R.R.-G., S.B.H., L.C.K., A.A., and M.O.S. wrote the manuscript with the input from all authors.

CONFLICTS OF INTEREST

Portions of this work were done under a Sponsored Research Agreement funded by Eisai, which manufactures and markets Eribulin mesylate under the brand name Halaven. D.W.C. is a current, and D.C. is a past, full-time employee of Eisai.

ACKNOWLEDGMENTS

We thank Bruce Littlefield for helpful discussions and Vincent Olieric and Meitian Wang for excellent technical assistance with the collection of X-ray data at beamlines X06DA and X06SA of the Swiss Light Source (Paul Scherrer Institut, Villigen, Switzerland). This work was financially supported by Eisai (to S.B.H., A.A., and M.O.S.), grants from the Swiss National Science Foundation (310030B_138659 and 31003A_166608 to M.O.S.), and a European Molecular Biology Organization Long-Term Fellowship to R.R.-G.

Received: April 11, 2015
Revised: March 15, 2016
Accepted: April 25, 2016
Published: June 16, 2016

REFERENCES

1. Gardner, M.K., Charlebois, B.D., Jánosi, I.M., Howard, J., Hunt, A.J., and Odde, D.J. (2011). Rapid microtubule self-assembly kinetics. Cell *146*, 582–592.
2. Coombes, C.E., Yamamoto, A., Kenzie, M.R., Odde, D.J., and Gardner, M.K. (2013). Evolving tip structures can explain age-dependent microtubule catastrophe. Curr. Biol. *23*, 1342–1348.
3. Zakharov, P., Gudimchuk, N., Voevodin, V., Tikhonravov, A., Ataullakhanov, F.I., and Grishchuk, E.L. (2015). Molecular and mechanical causes of microtubule catastrophe and aging. Biophys. J. *109*, 2574–2591.
4. Bowne-Anderson, H., Zanic, M., Kauer, M., and Howard, J. (2013). Microtubule dynamic instability: a new model with coupled GTP hydrolysis and multistep catastrophe. BioEssays *35*, 452–461.
5. Jordan, M.A., Kamath, K., Manna, T., Okouneva, T., Miller, H.P., Davis, C., Littlefield, B.A., and Wilson, L. (2005). The primary antimitotic mechanism of action of the synthetic halichondrin E7389 is suppression of microtubule growth. Mol. Cancer Ther. *4*, 1086–1095.
6. Smith, J.A., Wilson, L., Azarenko, O., Zhu, X., Lewis, B.M., Littlefield, B.A., and Jordan, M.A. (2010). Eribulin binds at microtubule ends to a single site on tubulin to suppress dynamic instability. Biochemistry *49*, 1331–1337.
7. Wilson, L., Lopus, M., Miller, H.P., Azarenko, O., Riffle, S., Smith, J.A., and Jordan, M.A. (2015). Effects of eribulin on microtubule binding and dynamic instability are strengthened in the absence of the βIII tubulin isotype. Biochemistry *54*, 6482–6489.
8. Prota, A.E., Bargsten, K., Zurwerra, D., Field, J.J., Díaz, J.F., Altmann, K.H., and Steinmetz, M.O. (2013). Molecular mechanism of action of microtubule-stabilizing anticancer agents. Science *339*, 587–590.
9. Prota, A.E., Magiera, M.M., Kuijpers, M., Bargsten, K., Frey, D., Wieser, M., Jaussi, R., Hoogenraad, C.C., Kammerer, R.A., Janke, C., and Steinmetz, M.O. (2013). Structural basis of tubulin tyrosination by tubulin tyrosine ligase. J. Cell Biol. *200*, 259–270.
10. Gigant, B., Wang, C., Ravelli, R.B., Roussi, F., Steinmetz, M.O., Curmi, P.A., Sobel, A., and Knossow, M. (2005). Structural basis for the regulation of tubulin by vinblastine. Nature *435*, 519–522.
11. Ranaivoson, F.M., Gigant, B., Berritt, S., Joullié, M., and Knossow, M. (2012). Structural plasticity of tubulin assembly probed by vinca-domain ligands. Acta Crystallogr. D Biol. Crystallogr. *68*, 927–934.
12. Alday, P.H., and Correia, J.J. (2009). Macromolecular interaction of halichondrin B analogues eribulin (E7389) and ER-076349 with tubulin by analytical ultracentrifugation. Biochemistry *48*, 7927–7938.
13. Bai, R., Nguyen, T.L., Burnett, J.C., Atasoylu, O., Munro, M.H., Pettit, G.R., Smith, A.B., 3rd, Gussio, R., and Hamel, E. (2011). Interactions of halichondrin B and eribulin with tubulin. J. Chem. Inf. Model. *51*, 1393–1404.
14. Dabydeen, D.A., Burnett, J.C., Bai, R., Verdier-Pinard, P., Hickford, S.J., Pettit, G.R., Blunt, J.W., Munro, M.H., Gussio, R., and Hamel, E. (2006). Comparison of the activities of the truncated halichondrin B analog NSC 707389 (E7389) with those of the parent compound and a proposed binding site on tubulin. Mol. Pharmacol. *70*, 1866–1875.
15. Ayaz, P., Ye, X., Huddleston, P., Brautigam, C.A., and Rice, L.M. (2012). A TOG:αβ-tubulin complex structure reveals conformation-based mechanisms for a microtubule polymerase. Science *337*, 857–860.
16. Pecqueur, L., Duellberg, C., Dreier, B., Jiang, Q., Wang, C., Plückthun, A., Surrey, T., Gigant, B., and Knossow, M. (2012). A designed ankyrin repeat

protein selected to bind to tubulin caps the microtubule plus end. Proc. Natl. Acad. Sci. USA *109*, 12011–12016.

17. Ravelli, R.B., Gigant, B., Curmi, P.A., Jourdain, I., Lachkar, S., Sobel, A., and Knossow, M. (2004). Insight into tubulin regulation from a complex with colchicine and a stathmin-like domain. Nature *428*, 198–202.
18. Prota, A.E., Bargsten, K., Diaz, J.F., Marsh, M., Cuevas, C., Liniger, M., Neuhaus, C., Andreu, J.M., Altmann, K.H., and Steinmetz, M.O. (2014). A new tubulin-binding site and pharmacophore for microtubule-destabilizing anticancer drugs. Proc. Natl. Acad. Sci. USA *111*, 13817–13821.
19. Chrétien, D., Metoz, F., Verde, F., Karsenti, E., and Wade, R.H. (1992). Lattice defects in microtubules: protofilament numbers vary within individual microtubules. J. Cell Biol. *117*, 1031–1040.
20. Bieling, P., Laan, L., Schek, H., Munteanu, E.L., Sandblad, L., Dogterom, M., Brunner, D., and Surrey, T. (2007). Reconstitution of a microtubule plus-end tracking system in vitro. Nature *450*, 1100–1105.
21. Mohan, R., Katrukha, E.A., Doodhi, H., Smal, I., Meijering, E., Kapitein, L.C., Steinmetz, M.O., and Akhmanova, A. (2013). End-binding proteins sensitize microtubules to the action of microtubule-targeting agents. Proc. Natl. Acad. Sci. USA *110*, 8900–8905.
22. Akhmanova, A., and Steinmetz, M.O. (2015). Control of microtubule organization and dynamics: two ends in the limelight. Nat. Rev. Mol. Cell Biol. *16*, 711–726.
23. Maurer, S.P., Bieling, P., Cope, J., Hoenger, A., and Surrey, T. (2011). GTPgammaS microtubules mimic the growing microtubule end structure recognized by end-binding proteins (EBs). Proc. Natl. Acad. Sci. USA *108*, 3988–3993.
24. Zhang, R., Alushin, G.M., Brown, A., and Nogales, E. (2015). Mechanistic origin of microtubule dynamic instability and its modulation by EB proteins. Cell *162*, 849–859.
25. Beltman, J.B., Marée, A.F., and de Boer, R.J. (2009). Analysing immune cell migration. Nat. Rev. Immunol. *9*, 789–798.
26. Maurer, S.P., Fourniol, F.J., Bohner, G., Moores, C.A., and Surrey, T. (2012). EBs recognize a nucleotide-dependent structural cap at growing microtubule ends. Cell *149*, 371–382.
27. Maurer, S.P., Cade, N.I., Bohner, G., Gustafsson, N., Boutant, E., and Surrey, T. (2014). EB1 accelerates two conformational transitions important for microtubule maturation and dynamics. Curr. Biol. *24*, 372–384.